

PAPER

# Optical setup for two-colour experiments at the low density matter beamline of FERMI

To cite this article: Paola Finetti *et al* 2017 *J. Opt.* **19** 114010

View the [article online](#) for updates and enhancements.

# Optical setup for two-colour experiments at the low density matter beamline of FERMI

Paola Finetti<sup>1</sup> , Alexander Demidovich<sup>1</sup>, Oksana Plekan<sup>1</sup>, Michele Di Fraia<sup>1</sup> , Riccardo Cucini<sup>1</sup> , Carlo Callegari<sup>1</sup> , Paolo Cinquegrana<sup>1</sup>, Paolo Sigalotti<sup>1</sup>, Rosen Ivanov<sup>1,6</sup>, Miltcho B Danailov<sup>1</sup> , Claudio Fava<sup>1</sup>, Giovanni De Ninno<sup>1,2</sup>, Marcello Coreno<sup>3</sup>, Cesare Grazioli<sup>3</sup>, Raimund Feifel<sup>4</sup>, Richard J Squibb<sup>4</sup>, Tommaso Mazza<sup>5</sup>, Michael Meyer<sup>5</sup> and Kevin C Prince<sup>1,7</sup> 

<sup>1</sup> Elettra-Sincrotrone Trieste, I-34149 Basovizza, Trieste, Italy

<sup>2</sup> Laboratory of Quantum Optics, University of Nova Gorica, 5001 Nova Gorica, Slovenia

<sup>3</sup> ISM-CNR, Laboratorio Elettra, I-34149 Basovizza, Trieste, Italy

<sup>4</sup> Department of Physics, University of Gothenburg, SE-41258 Gothenburg, Sweden

<sup>5</sup> European XFEL GmbH, D-22869 Schenefeld Hamburg, Germany

E-mail: [Prince@Elettra.Eu](mailto:Prince@Elettra.Eu)

Received 14 July 2017, revised 12 September 2017

Accepted for publication 28 September 2017

Published 23 October 2017



CrossMark

## Abstract

The low density matter beamline of the free electron laser facility FERMI is dedicated to the study of atomic, molecular and cluster systems, and here we describe the optical setup available for two-colour experiments. Samples can be exposed to ultrashort pulses from a Ti:Sapphire source (fundamental, or second or third harmonic), and ultrashort light pulses of FERMI in the EUV/soft x-ray region with a well-defined temporal delay, and negligible jitter (<10 fs) compared to the pulse durations (40–100 fs). Detection schemes available include electron, ion and optical spectroscopy. The majority of experiments using this apparatus are pump-and-probe, where either wavelength can be pump or probe, but the system is also useful for other techniques, such as multi-photon spectroscopy, cross-correlation measurements and alignment of molecules in space.

Keywords: free electron laser, two colour spectroscopy, pump-probe

(Some figures may appear in colour only in the online journal)

## 1. Introduction

The interactions of radiation with matter, where a light pulse excites a system and a second pulse with a well-defined temporal delay probes the excited states, are at the heart of laser-based studies of dynamics. With the advent of short-wavelength free electron laser (FEL) sources with unprecedented brilliance and intensity over a wide wavelength range, dynamical studies have become possible with chemical selectivity, because core levels can be probed. FERMI operates in the range 4–100 nm and its seeded mode of operation achieves high and stable energy per pulse in a narrow

bandwidth, a high degree of longitudinal coherence, full wavelength and polarization tunability, and pulse duration of the order of 100 fs duration or less [1, 2]. These features make FERMI an ideal tool for the study of the dynamics of both resonant and non-resonant excitations.

The low density matter (LDM) beamline at FERMI is dedicated to the study of rarefied materials such as atomic, molecular and cluster systems. Its modular end-station [3] can host a variety of LDM sources, and provides simultaneous electron and ion spectroscopy by means of a velocity map imaging detector and ion time of flight spectrometer. These spectrometers can be used in conjunction with a photon scattering detector for structural studies of clusters. A magnetic bottle spectrometer, named FERMI-FELCO, has

<sup>6</sup> Now at: Deutsches Elektronen-Synchrotron, D-22607 Hamburg, Germany.

<sup>7</sup> Author to whom any correspondence should be addressed.

also been employed at LDM [4, 5], and a spectrometer for x-ray emission experiments is also available [6].

The LDM beamline is provided with a setup to allow two-colour experiments where the FEL light is combined with the fundamental (or second or third harmonic) wavelength of a Ti:Sapphire laser. Optical + FEL two-colour experiments constitute a large part of the LDM experimental activity, with new experiments being proposed at each call for beamtime proposals. Examples of the outcome of this experimental activity are the observation and utilization of circular dichroism in the two-colour photoemission of He [7–9], studies of the dynamics of interatomic Coulombic decay [10, 11], cross-correlation measurements of pulse duration [12], and optical alignment of molecules [13].

One of the most prominent features of the pump-and-probe system available at FERMI is the precise synchronization between the FEL and the optical laser [14, 15]. This result is based on a scheme where a fraction of the infrared (IR) Ti:Sapphire amplifier pulse used to trigger the FEL emission is separated and transported to the FERMI experimental stations. This pulse, hereafter referred to as seed laser for users (SLU), is used as an external pulse in the FERMI two-colour setups. In this scheme, the timing of both the FEL pulse and the SLU pulse comes from a common mode-locked oscillator, allowing the generation of FEL/optical laser pulse pairs with very low mutual timing jitter. The IR laser beam transport from the seed laser to the experimental stations has been carefully designed to obtain a very high pointing stability (and therefore very low path-length fluctuations), and in addition a piezo tip-tilt based feedback system is used for long term beam pointing stabilization [14]. As a result, and despite the 150 m long transport section, the relative timing jitter between optical laser pulses and FEL pulses measured at the experimental stations is less than 10 fs rms [15]. With such low timing jitter, post-processing of the data to establish the relative arrival time of the two laser pulses (usual at unseeded FELs) is unnecessary.

In this paper, we provide a detailed description of the main features of the layout of the system for coupling the optical laser with the FEL light, together with the principal methods employed to prepare two-colour experiments on LDM. Here, we discuss only the case where one of the two colours is optical and one is FEL light; at FERMI it is also possible to perform a wide range of experiments where both colours are generated by the FEL [16–19].

## 2. Laser setup

The FERMI seed pulse starts from a femtosecond Ti:Sapphire oscillator (Vitara, Coherent) which is locked to the reference timing signal which determines repetition rate, and is distributed over the facility [20]. Originally, the seed laser system had a single Ti:Sapphire based amplifier consisting of a chirped-pulse regenerative amplifier and a single pass amplifier delivering pulses with an energy of up to 6 mJ and a duration of about 100 fs with a central wavelength around 785 nm. The main portion of the amplifier output pulse was

used to pump the optical parametric amplifier (OPA) generating the tunable UV pulses used for FEL seeding. The remaining part of the IR pulse was used as a SLU pulse and sent to the experimental stations. The setup has recently been upgraded to a more flexible version, where an additional regenerative amplifier, seeded by the same Vitara oscillator, has been added, providing more flexible timing and higher IR pulse energy for the SLU. Further improvements are planned in 2018.

The beam propagation to the beamlines is based on relay imaging and most of the path is in low vacuum, preserving the very good beam quality. To avoid nonlinear effects, the pulses sent to the beam transport are stretched by introducing a negative linear chirp. The chirp is then compensated at the delivery point in the experimental hall by a compact transmission grating pulse compressor. The final duration of the pulse can be varied in the range 60–1000 fs and adjusted to the needs of the experiment. The SLU pulse is delivered to all the experimental stations currently operating at FERMI, each station having a separate setup for final beam preparation and transport to the experimental station.

## 3. SLU setup at LDM

The SLU optical setup at LDM includes two optical breadboards containing the components for beam manipulation, harmonic generation, diagnostics and introduction into the chamber. The breadboards are covered with protective boxes and flushed with nitrogen to prevent dust contamination of the optical components. A layout of the full LDM setup is presented in figure 1. CCD1 controls the position and spatial parameters of the incoming beam after the vacuum window W1 and is incorporated in the beam transport system. The motorized mirror mount MM1 and CCD2 allow control of the laser beam direction of propagation on the optical breadboard. An optical attenuator, made of a half waveplate ( $\lambda/2@780$  nm) WP1 and two thin film polarizers (PL1, PL2), allows adjustment of the exact pulse energy delivered to the interaction region. A translation stage TS1 (PI M403.8PD) provides a variable pulse delay relative to the FEL pulse in the range of  $\pm 660$  ps with minimum step of 1.6 fs.

The setup includes a high-bandwidth copper coaxial cable based antenna positioned directly at the recombination position of the laser and the FEL beam which allows an initial coarse estimate of the time delay between the two pulses by means of a fast oscilloscope (typical resolution of the pulse temporal position less than 50 ps). The fast photodiode signal is used as a trigger source for the oscilloscope in this case. A compact single-shot auto-correlator is installed for diagnostics of the input IR pulse duration.

It is possible to convert the IR laser pulse to the 390–396 nm range or to the 261–264 nm range by generating the second or third harmonic in consecutive BBO crystals (labelled SH and TH). An additional calcite time delay plate TDP and a double wavelength waveplate ( $\lambda/2@780$  nm,  $\lambda@390$  nm) WP2 are inserted in the beam path. The interference filter F1 is used to select second harmonic emission

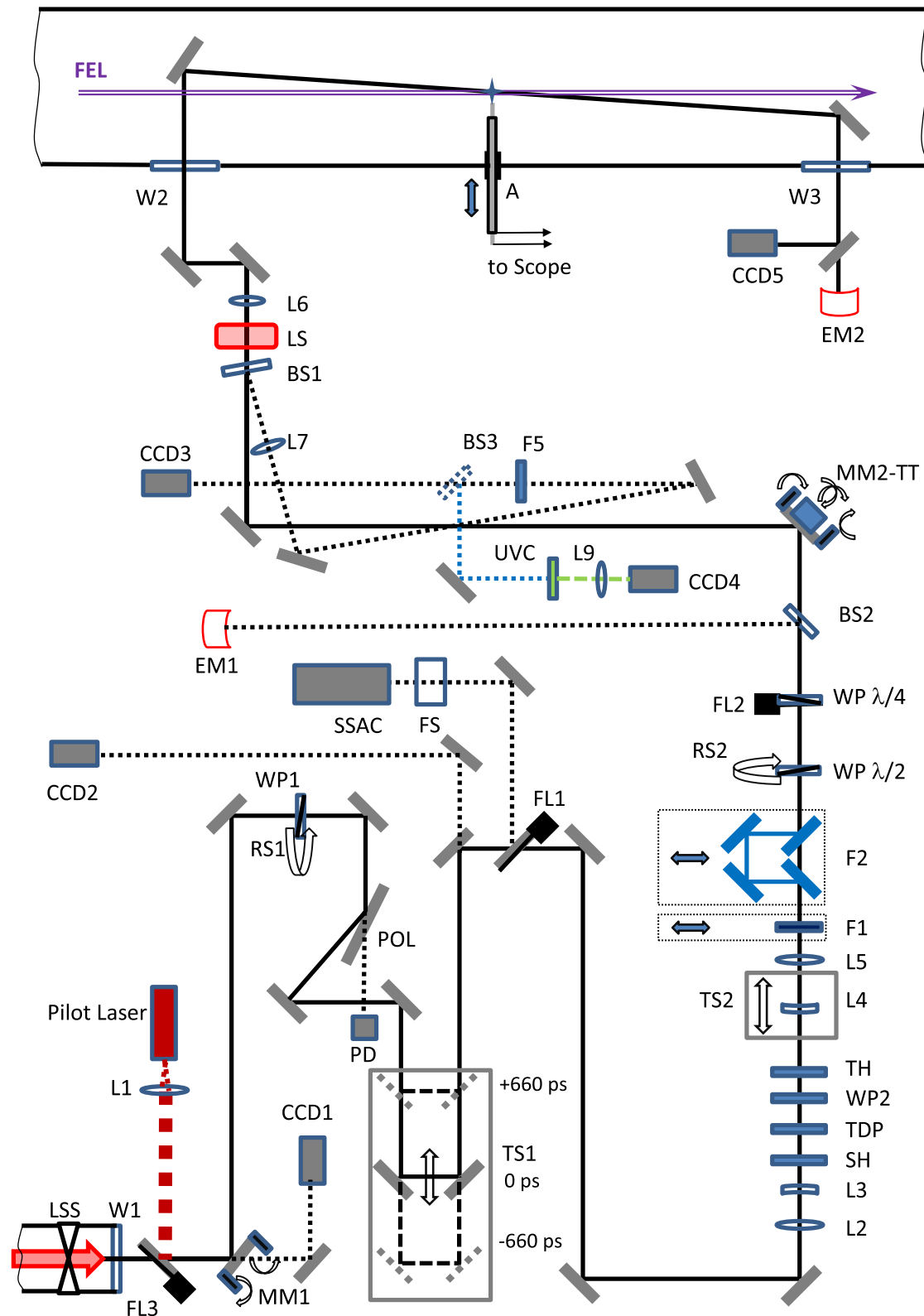


**Figure 1.** Optical layout of the SLU at the LDM experimental station. FEL: beam from FERMI. Optical elements and actuators are labelled as follows, where  $n$  is a number. A: antenna. BS $n$ : beam sampler. CCD $n$ : CCD camera. EM $n$ : energy meter. F $n$ : filter. FL $n$ : flipper. FS: fused silica substrate. L $n$ : lens. LSS: main laser shutter. LS: additional laser shutter. MM $n$ : motorized mirror mount. PD: photodiode. POL: polarizer. RS $n$ : rotation stage. SH: second harmonic crystal. TDP: time delay plate. TH: third harmonic crystal. TS $n$ : translation stage. TT: tip-tilt. UVC: UV to visible converter. W $n$ : window. WP $n$ : half-wave plate at 800 nm. WP  $\lambda/4$  and WP  $\lambda/2$ : half or quarter wave plates (depending on the requested polarization state) for the wavelength in use. SSAC: compact single-shot auto-correlator.

**Table 1.** Current main parameters of the SLU at the LDM end-station.

Parameter	Value
Optical pulse wavelength	785–795 nm 390–396 nm 261–264 nm
Maximum pulse energy at the interaction point	2 mJ@790 nm 700 $\mu$ J@395 nm 150 $\mu$ J@263 nm
Pulse energy stability (rms)	<0.5%@790 nm <1.0%@395 nm <1.0%@263 nm
Pulse length at 790 nm (FWHM)	60–1000 fs
Pulse repetition rate	1–10 Hz, 50 Hz
Timing jitter relative to FEL (rms)	<10 fs
Scan range pulse delay relative to FEL	–660... +660 ps
Minimum delay step	1.6 fs
Beam diameter at region of interaction (at level $1/e^2$ )	80–500 $\mu$ m
Beam position stability (rms)	<5 $\mu$ m

when required. A set of four mirrors with HR@260 nm, HT@390 nm and HT@780 nm is used as a filter (F2) to select only the TH UV emission. Polarization state control of the laser light arriving in the chamber is performed by using a half-wave waveplate (WP  $\lambda/2$ ) mounted on the rotation stage RS2 and a quarter-wave waveplate (WP  $\lambda/4$ ) mounted on the flipper FL2. Both waveplates are selected for the wavelength range in use. This design provides the possibility to set linear polarization with the desired orientation, or left/right circular polarization for all operating wavelengths. The energy meter heads EM1 and EM2 allow monitoring of the pulse energy. The optical system includes three lenses L4, L5, L6 that focus the laser beam in the interaction plane down to a spot diameter of 80  $\mu$ m ( $1/e^2$  diameter). The lens L4 is mounted on a motorized translation stage TS2 (Standa 8MT173-25), which allows one to keep the focus position when switching between the above mentioned wavelengths of operation or to increase the beam diameter up to 500  $\mu$ m. The camera CCD3 is used as a virtual focal point and allows monitoring of the beam size and position of the fundamental and second harmonic beam, while the same function for the third harmonic beam is performed by the UV–visible converter UVC and CCD4. The motorized mount M2-TT, which incorporates an active piezo tip-tilt mirror, allows scanning of the beam position with high accuracy, and is also used by a pointing stabilization system with beam position stability (rms) of less than 5  $\mu$ m. The IR pilot laser is installed on the breadboard to assist the preparation of the setup when the SLU is unavailable. The main design parameters of the current setup are listed in table 1.

FERMI typically operates at 50 or 10 Hz repetition rate of the electron accelerator; the former is the default, except at short wavelengths (high electron energies), when 10 Hz is used. The rate of light pulses can be reduced by periodically skipping the corresponding seed laser pulses. 1 Hz is a standard option with instruments that have long read-out times, such as the wavefront sensor used for setting the focussing of the FEL beam. If needed, the SLU can be set to have a

different repetition rate from the FEL by using a different trigger repetition rate of the two amplifiers, but it should be noted that the data acquisition system runs at the accelerator repetition rate. Thus it is not useful to set the SLU to a higher rate. In addition, a shutter inside the laser breadboard allows control of the repetition rate of the SLU pulses entering the LDM chamber in the 10–1 Hz range.

#### 4. FEL-SLU recombination

The recombination between the FEL and the SLU pulses is carried out in the beamline section depicted in figure 2. The recombination mirror has a coating optimized for the three wavelengths delivered by the SLU and placed in ultra-high vacuum (UHV). The recombination mirror is positioned after the last optical component of the LDM beamline for FEL transport [21] which is the second of a pair of active KB mirrors. The distance between the recombination mirror and the interaction region is about 500 mm. The SLU beamline section in air and the UHV section are separated by a 3 mm thick fused silica window with antireflective coating for the three wavelengths of the SLU. The bottom edge of the recombination mirror is 3 mm above the top edge of the FEL beam edge (considering the beam divergence at the longest FEL wavelength). With this geometry, the FEL and SLU beams recombine at the interaction region with an almost collinear geometry, at an angle of  $0.6^\circ$ . The recombination mirror is mounted on an adaptor that is directly connected to a manually actuated STANDA (5VDOM-1) kinematic mount with 2 arcsec sensitivity, conditioned to make it UHV compatible. Via a system of rotary drives, the adjustment of the tip-tilt position can be done in UHV. The mirror support assembly is mounted on a jacking stage type of linear drive (VG thermionics) to allow variations of the coupling geometry. Future upgrades of the system will include the use of a hollow recombination mirror for a fully collinear geometry between the FEL and the SLU. The recombination mirror

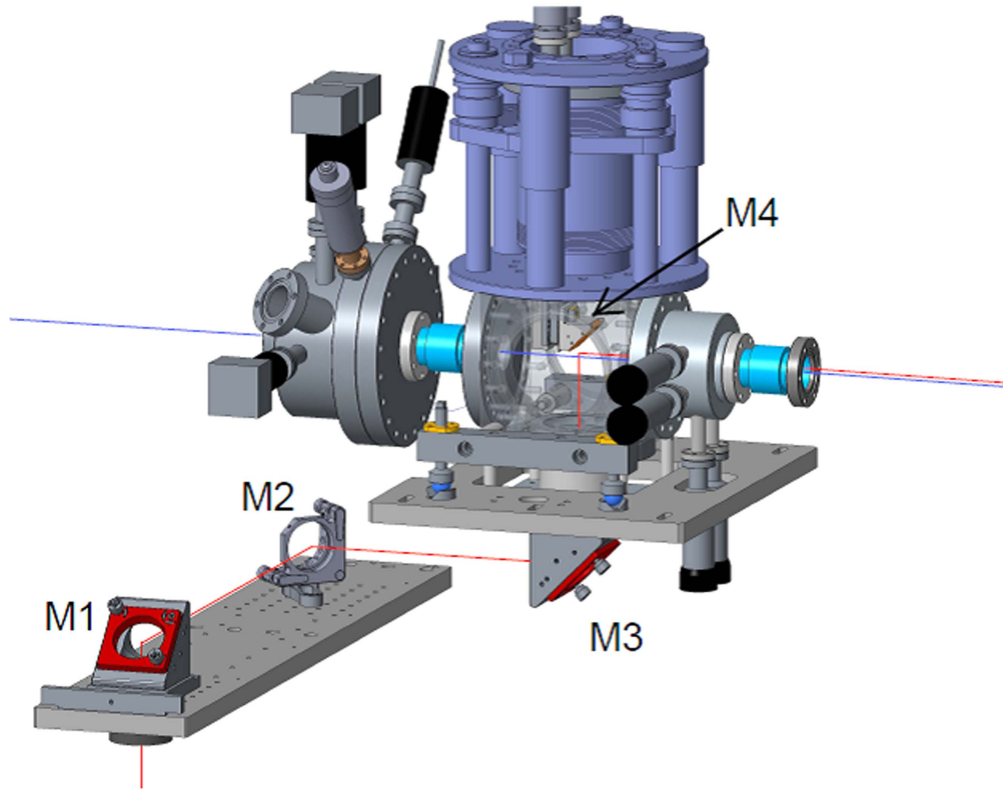


**Figure 2.** Recombination mirror section of the SLU beam transport system. With respect to figure 1, the mirrors have been numbered, and the elements BS1, LS, L6 between M1 and M2 have been omitted. The two beams emerge on the right at an angle of  $0.6^\circ$  with respect to one another.

section is pumped by a combination of ion and turbomolecular pumps, and the latter is mechanically decoupled from the vacuum vessel by means of an edge-welded bellows. Before and after the recombination mirror, FEL beam defining apertures are available in order to reduce the amount of stray light.

## 5. Standard setup operations of the SLU

Under normal operation, the system alignment does not require major variations but only fine adjustment of the SLU beam positioning, which is carried out by means of the piezo-driven tip-tilt actuator used to optimize the FEL and SLU spatial overlap. This adjustment is made necessary primarily due to small variations of the FEL pointing from one alignment session to the next (causing positional movements of the order of a few tens of micron), and which may include optimization of the active optics. An initial adjustment of the spatial overlap is carried out by optical methods, where the footprint of the two beams at the interaction region is retrieved after projecting the beams onto a YAG screen (for visualizing UV, green and XUV light) which is in direct contact with a ground glass plate (for visualizing 785 nm light). This diagnostic screen is inserted for this check and then retracted.

The fine adjustment of the FEL and SLU spatial and temporal overlap is carried out by means of spectroscopic

methods, usually with noble gas targets [8]. The sample is excited to a long lived, neutral resonant state by the FEL beam, and then ionized by the SLU light; the ions or electrons are the signal used for optimization. Both He and Ne are frequently used on LDM for this type of measurement, and in the following, we take He as an example, but a similar procedure can be followed using the resonances of Ne. In a typical He based pump and probe measurement, one FEL photon excites He from the ground state to a  $1snp$  resonant state ( $\text{He} + h\nu_{\text{FEL}} \rightarrow \text{He } 1snp$ ). The quantum number  $n$  defining the transition is typically chosen so that one SLU photon is sufficient to ionize the excited state ( $\text{He } 1snp + h\nu_{\text{SLU}} \rightarrow \text{He}^+ + e^-$ ). For example, the He  $1s5p$  resonance at 24.046 eV is often used. Multiphoton processes ( $\text{He } 1snp + mh\nu_{\text{SLU}} \rightarrow \text{He}^+ + e^-$ , where  $m$  is an integer) may occur, depending on the SLU intensity (see figure 3). The ionization of He following two-colour photon absorption can be monitored by photoemission spectroscopy or by ion yield spectroscopy. If the lifetime of the resonant excited state is long compared to the delay  $\tau$  between the FEL and SLU pulses, the intensity of the photoemission or the ion yield (when only single photon processes occur)  $I_{\text{spec}}$  can be written:

$$I_{\text{spec}}(\tau) = \int_{-\infty}^{\infty} dt I_{\text{FEL}}(t - \tau) \int_t^{\infty} dt' I_{\text{SLU}}(t'). \quad (1)$$

The result is that  $I_{\text{spec}}$  as a function of the delay is a step-like function broadened by the convolution of the temporal profiles of the two pulses, and the delay time  $t_0$  corresponding to

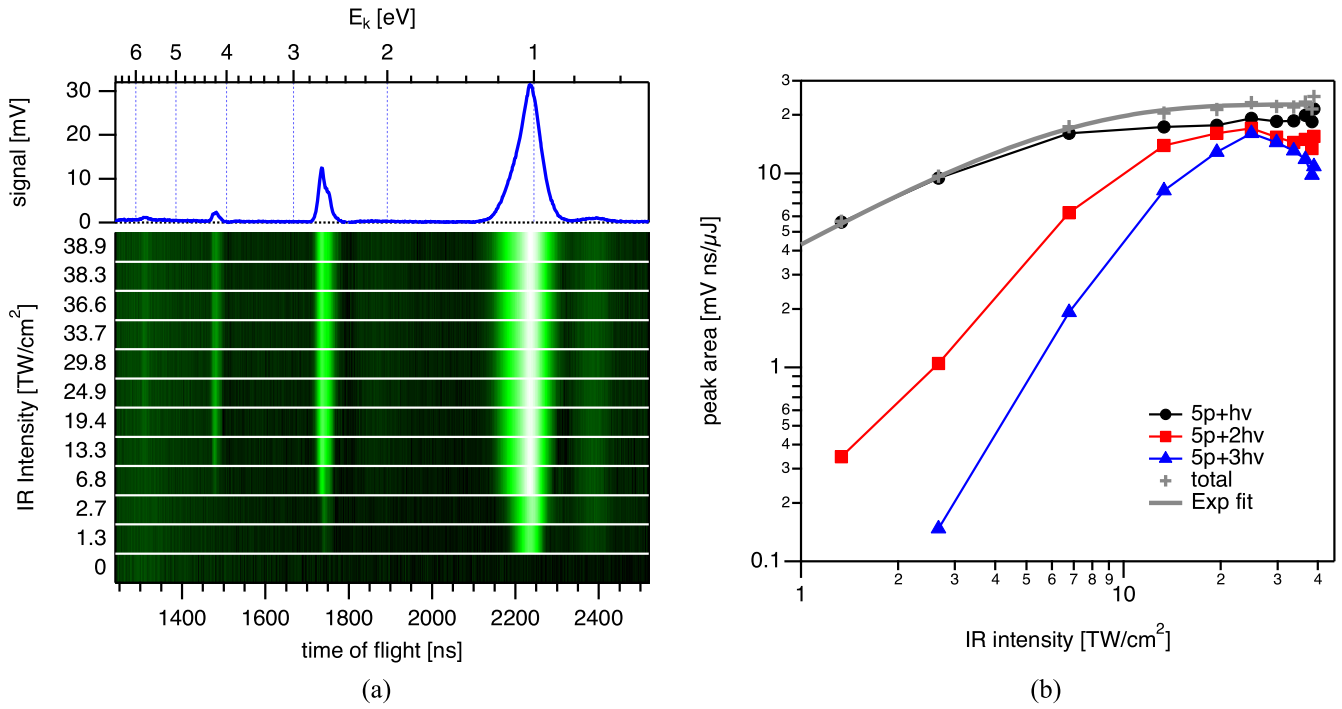


**Figure 3.** (a) Photoemission data from the two-colour ionization of He via the  $1s5p$  resonance ( $\text{He } 1s5p + mh\nu_{\text{SLU}} \rightarrow \text{He}^+ + e^-$ ) as a function of the infrared (IR) intensity of the SLU ( $\lambda = 784 \text{ nm}$ ). The colour scale is compressed to enhance contrast. Top curve: spectrum at maximum IR intensity. (b) Integrated photoemission intensity as a function of IR intensity. Symbols: +, all electrons (grey, with fitted curve): ● two photons (black); ■ FEL + 2 IR photons (red); ▲ FEL + 3 IR photons (blue). The signals have been normalized to the FEL pulse energy in  $\mu\text{J}$ .

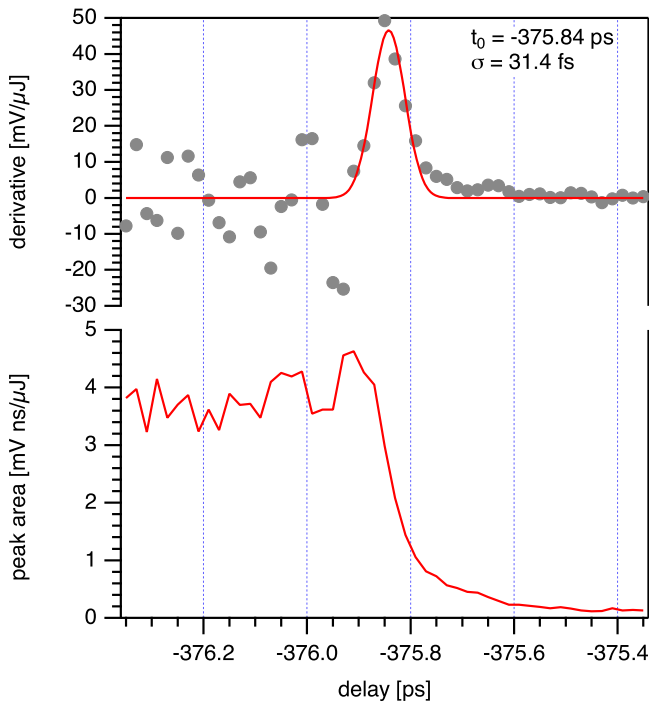


**Figure 4.** Lower curve: ion yield versus delay of the two-photon, two-colour ionization of He via the  $1s5p$  resonant state. Upper curve: grey dots, derivative of the data; red line; Gaussian fit of the data. The time scale origin is arbitrary, and in this case  $t_0$  was found at 375.84 ps.

temporal overlap is given by the inflection point of this curve (see figure 4). Note that in the temporal overlap region, also two-colour, two-photon non-resonant photoemission can occur [22], therefore equation (1) provides only an approximation of the full cross-correlation curve, that should however preserve the position of  $t_0$ . The lifetimes of the He  $1snp$  resonant states (1.71 ns to 59.8 ns, for  $n = 3$  and 10) are longer than the full range delay available at the end-station [23], so that these levels are suitable for a full range search for  $t_0$ .

Figure 3 shows the intensity of the photoemission from He due to resonant excitation by the FEL, plus 1 to 3 IR photons. At lower SLU intensities ( $< 3 \text{ TW cm}^{-2}$ ), the intensities of the first three peaks (absorption of 1, 2 and 3 IR photons) are approximately linear, quadratic and cubic respectively in IR power. At higher power, all peaks saturate. The weak feature at 2400 ns flight time is an electronic artefact due to ringing. This method can be used for all three available SLU wavelengths.

The short wavelength light of FERMI is produced by selecting a seed wavelength, and a higher harmonic of that wavelength. The desired wavelength can be selected by tuning the seed, or selecting a harmonic or both. If the above procedure is followed at a given harmonic, and the seed wavelength is not changed, the value of  $t_0$  remains valid when another harmonic is selected (increments of about 5 eV). The reason is that when the FEL wavelength is changed from one

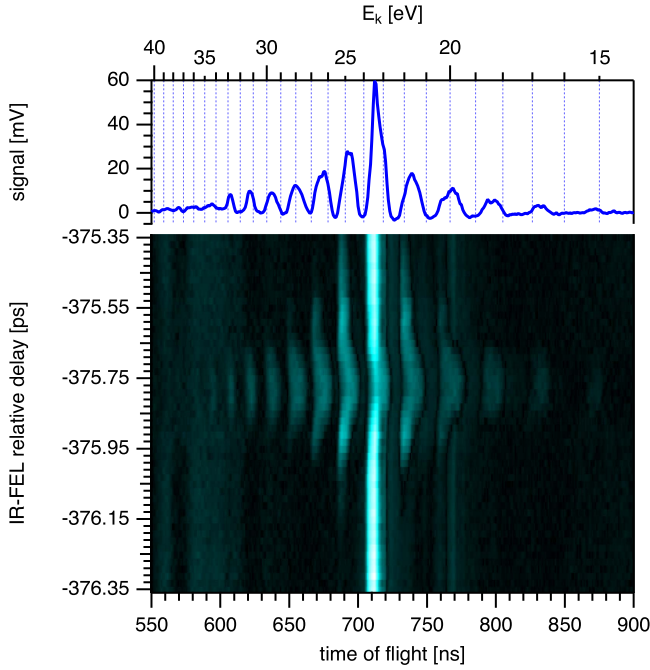


**Figure 5.** Lower panel: intensity of the sidebands, measured with the FELCO magnetic bottle spectrometer as a function of the delay between the IR and FEL pulses. The colour scale is compressed to enhance contrast.  $h\nu_{\text{FEL}} = 48.1$  eV,  $h\nu_{\text{SLU}} = 1.59$  eV. The kinetic energy of the sidebands and the main line are  $KE_{\text{SB}}$  and  $KE_{\text{ML}}$ ;  $KE_{\text{SB}} - KE_{\text{ML}} = \pm m h\nu_{\text{SLU}}$ , where  $m$  is the number of SLU photons that are absorbed or emitted. Upper panel: spectrum at maximum time overlap on a linear electron time-of-flight scale (lower axis). Upper axis (kinetic energy scale) is calibrated by fitting the positions of the peaks.

harmonic to another, while other parameters such as the seed wavelength are kept constant, the trajectory of the electrons in the FERMI undulators is lengthened or shortened by only a small amount, of the order of the wavelength of the light. Thus the time of arrival of different harmonics differs by a time of the order of the period of the light, which is in the attosecond range.

We note that resonances of the He ion have also been used. These resonances are generally at shorter wavelengths than those of the neutral atom, extending the range of FEL wavelengths that can be probed directly with this resonant method. When the ion is used rather than the neutral, usually multiphoton ionization by the SLU photons is required, as excited ions often lie energetically well below the threshold for second ionization. For example, if the  $3p$  excited state of  $\text{He}^+$  is used, then four IR photons are necessary to ionize it, as the state lies 6.05 eV below the ionization threshold.

For FEL wavelengths that are seeded at different wavelengths, the variations of the OPA setup of FERMI may change the delay. This is because the geometry of the light path inside the OPA which provides the seed pulse is wavelength dependent, thus affecting the FEL beam. This is to a large extent automatically compensated by available look-up tables. To achieve maximum possible accuracy of  $t_0$ , once spatial and temporal overlap have been established at the resonance wavelength,  $t_0$  is remeasured at the non-resonant wavelength with a method that is wavelength independent.

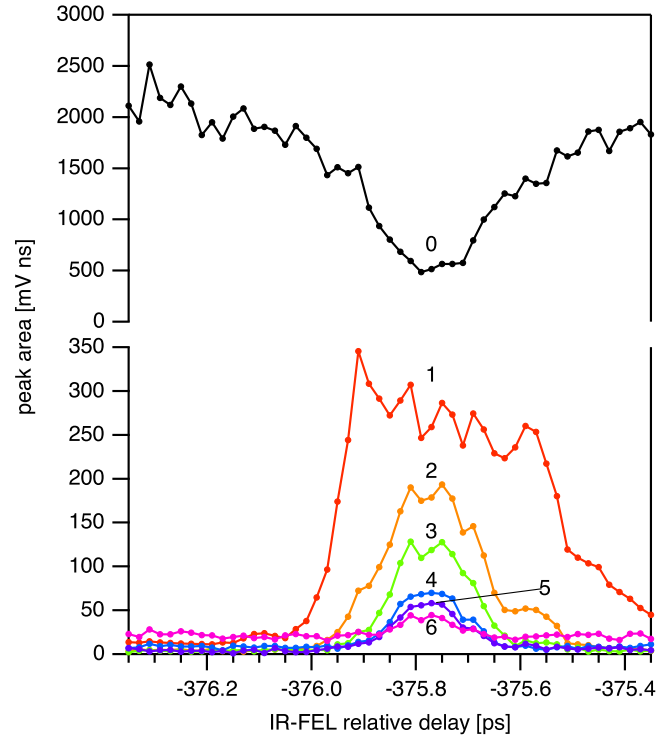


**Figure 6.** Cross-correlation curve of the main line and six of the positive sidebands shown in figure 5. Numbering refers to the number of IR photons absorbed, for example 0 indicates the main line intensity, 1 the first sideband, etc. The main line is depleted in the presence of IR radiation and therefore shows a reduction of intensity for overlap.

Cross-correlation from sidebands measured in photoemission is a suitable scheme. In this case, the FEL photon energy is set above the ionization potential of the atom, and near the main line, satellite peaks appear that are due to the simultaneous absorption or stimulated emission of SLU photons, figure 5. If the two light pulses do not overlap, no signal is produced. Thus this method is unsuitable for wide searches, but is effective when a good approximation to  $t_0$  is known. Note in figure 5 that for exact temporal overlap, the main line and sidebands are shifted to lower kinetic energy by about 1 eV due to the ponderomotive potential of the IR radiation [24]. This value is consistent with the intensity of the IR field, and the determination of  $t_0$  is not affected and remains accurate.

The intensity  $I_{\text{SB}}$  of the sidebands as a function of the delay between the FEL and the SLU is given by

$$I_{\text{SB}}(\tau) \propto \int_{-\infty}^{\infty} I_{\text{FEL}}(t - \tau) I_{\text{SLU}}^m(t) dt, \quad (2)$$

where  $m$  is the number of absorbed or emitted photons. In writing equation (2), we assume a SLU intensity which is sufficiently low to avoid saturation of the sideband signal. A cross correlation curve obtained from data, such as that in figure 5, is shown in figure 6. Cross-correlation from sidebands has also been used to measure the duration of the FERMI pulse [12].

With the power available at the SLU, the sidebands method has proved to be most effective using IR light rather than the second or third harmonics. This is because the

cross-section for the first sideband scales as the inverse fourth power of the frequency of the dressing field for our experimental conditions [25]. Both the resonant and non-resonant processes can be used to set up the SLU even with the high energy source FERMI FEL-2 (operating range 4–20 nm).

## 6. Conclusions

We have provided a detailed description of the pump-and-probe set-up available at the LDM beamline, operating at the seeded FEL facility FERMI. By recombining the FEL with a laser pulse derived from the same Ti:Sapphire oscillator used to seed the FEL, this setup provides virtually jitter free external laser pulses to the LDM end-station. Three different wavelengths are available, the fundamental at 790 nm, and the second and third harmonics. This setup is designed to match all the major requirements for experiments carried out at FERMI, polarization control included. By means of gas phase measurements, the SLU spatio-temporal overlap between the FEL and the external laser can be easily and quickly tuned. This experimental set-up is available with both the FERMI sources FEL-1 and FEL-2.

## Acknowledgments

RF acknowledges financial support from the Swedish Research Council and the Knut and Alice Wallenberg Foundation, Sweden.

## ORCID iDs

Paola Finetti  <https://orcid.org/0000-0001-5857-2675>  
 Michele Di Fraia  <https://orcid.org/0000-0001-8102-0799>  
 Riccardo Cucini  <https://orcid.org/0000-0001-8516-1409>  
 Carlo Callegari  <https://orcid.org/0000-0001-5491-7752>  
 Miltcho B Danailov  <https://orcid.org/0000-0002-1888-1331>  
 Kevin C Prince  <https://orcid.org/0000-0002-5416-7354>

## References

- [1] Allaria E, Callegari C, Cocco D, Fawley W M, Kiskinova M, Masciovecchio C and Parmigiani F 2010 The FERMI@Elettra free-electron-laser source for coherent x-ray physics: photon properties, beam transport system and application *New J. Phys.* **12** 075002
- [2] Allaria E *et al* 2013 Two-stage seeded soft-x-ray free-electron laser *Nat. Photon.* **7** 913
- [3] Lyamayev V *et al* 2013 A modular end-station for atomic, molecular, and cluster science at the low density matter beamline of FERMI@Elettra *J. Phys. B: At. Mol. Opt. Phys.* **46** 164007
- [4] Frasinski L J *et al* 2013 Dynamics of hollow atom formation in intense x-ray pulses probed by partial covariance mapping *Phys. Rev. Lett.* **111** 073002
- [5] Mucke M *et al* 2015 Covariance mapping of two-photon double core hole states in C<sub>2</sub>H<sub>2</sub> and C<sub>2</sub>H<sub>6</sub> produced by an x-ray free electron laser *New J. Phys.* **17** 073002
- [6] Poletto L, Frassetto F, Miotti P, Di Cicco A, Finetti P, Grazioli C, Iesari F, Kivimäki A, Stagira S and Coreno M 2014 Spectrometer for x-ray emission experiments at FERMI free-electron-laser *Rev. Sci. Instrum.* **85** 103112
- [7] Mazza T *et al* 2014 Determining the polarization state of an extreme ultraviolet free-electron laser beam using atomic circular dichroism *Nat. Commun.* **5** 3648
- [8] Mazza T *et al* 2016 Angular distribution and circular dichroism in the two-colour XUV + NIR above-threshold ionization of helium *J. Mod. Opt.* **63** 367
- [9] Ilchen M *et al* 2017 Circular dichroism in multiphoton ionization of resonantly excited He<sup>+</sup> ions *Phys. Rev. Lett.* **118** 013002
- [10] Iablonskyi D *et al* 2016 Slow interatomic Coulombic decay of multiply excited neon clusters *Phys. Rev. Lett.* **117** 276806
- [11] Takanashi T *et al* 2017 Time-resolved measurement of interatomic Coulombic decay induced by two-photon double excitation of Ne<sub>2</sub> *Phys. Rev. Lett.* **118** 033202
- [12] Finetti P *et al* 2017 Pulse duration of seeded free-electron lasers *Phys. Rev. X* **7** 021043
- [13] Di Fraia M *et al* 2017 Impulsive laser-induced alignment of OCS molecules at FERMI *Phys. Chem. Chem. Phys.* **19** 19733
- [14] Cinquegrana P, Cleva S, Demidovich A, Gaio G, Ivanov R, Kurdi G, Nikolov I, Sigalotti P and Danailov M B 2014 Optical beam transport to a remote location for low jitter pump-probe experiments with a free electron laser *Phys. Rev. Spec. Top. Accel. Beams* **17** 040702
- [15] Danailov M B *et al* 2014 Towards jitter-free pump-probe measurements at seeded free electron laser facilities *Opt. Express* **22** 12869
- [16] Allaria E *et al* 2013 Two-colour pump-probe experiments with a twin-pulse-seed extreme ultraviolet free-electron laser *Nat. Commun.* **4** 2476
- [17] Roussel E, Ferrari E, Allaria E, Penco G, Di Mitri S, Veronese M, Danailov M, Gauthier D and Giannessi L 2015 Multicolor high-gain free-electron laser driven by seeded microbunching instability *Phys. Rev. Lett.* **115** 214801
- [18] Prince K C *et al* 2016 Coherent control with a short-wavelength free electron laser *Nat. Photon.* **19** 176
- [19] Iablonskyi D *et al* Observation and control of laser-enabled Auger decay *Phys. Rev. Lett.* **119** 073203
- [20] Ferianis M, Borga A, Bucconi A, Pavlovic L, Predonzani M and Rossi F 2011 All-optical femtosecond timing system for the FERMI@Elettra FEL *33rd Int. Free Electron Laser Conf. 2011 (Shanghai, China)* pp 641–7
- [21] Svetina C *et al* 2015 The low density matter (LDM) beamline at FERMI: optical layout and first commissioning *J. Synchrotron Radiat.* **22** 538
- [22] Mondal S *et al* 2013 Photoelectron angular distributions in infrared one-photon and two-photon ionization of FEL-pumped Rydberg states of helium *J. Phys. B: At. Mol. Opt. Phys.* **46** 20
- [23] Žitnik M, Stanič A, Bučar K, Lambourne J G, Penent F, Hall R I and Lablanquie P 2003 Lifetimes of n<sup>1</sup>P states in helium *J. Phys. B: At. Mol. Opt. Phys.* **36** 4175
- [24] Bucksbaum P H, Freeman R R, Bashkansky M and McIlrath T J 1987 Role of the ponderomotive potential in above-threshold ionization *J. Opt. Soc. Am. B* **4** 760
- [25] Maquet A and Taïeb R 2007 Two-colour IR+XUV spectroscopies: the ‘soft-photon approximation’ *J. Mod. Optics* **54** 1847